AGU PUBLICATIONS

JGR

Journal of Geophysical Research: Solid Earth

RESEARCH ARTICLE
10.1002/2017JB014231

Key Points:
- Kinetics of serpentinization were studied experimentally
- Compared to olivine, peridotite shows much faster rates of serpentinization
- Pyroxene and spinel released Al and Cr that greatly promote olivine serpentinization

Supporting Information:
- Supporting Information S1

Correspondence to:
R. Huang and W. Sun,
rfhuang@gig.ac.cn;
weidongsun@gig.ac.cn

Citation:
Huang, R., M. Song, X. Ding, S. Zhu, W. Zhan, and W. Sun (2017), Influence of pyroxene and spinel on the kinetics of peridotite serpentinization, *J. Geophys. Res. Solid Earth*, *122*, 7111–7126, doi:10.1002/2017JB014231.

Received 22 MAR 2017
Accepted 14 AUG 2017
Accepted article online 17 AUG 2017
Published online 14 SEP 2017

Influence of pyroxene and spinel on the kinetics of peridotite serpentinization

Ruifang Huang[1,2], Maoshuang Song[3], Xing Ding[3], Sanyuan Zhu[4], Wenhuan Zhan[2], and Weidong Sun[5,6,7]

[1]Key Laboratory of Mineralogy and Metallogeny, Guangzhou Institute of Geochemistry, Chinese Academy of Sciences, Guangzhou, China, [2]Key Laboratory of Ocean and Marginal Sea Geology, South China Sea Institute of Oceanology, Chinese Academy of Sciences, Guangzhou, China, [3]State Key Laboratory of Isotope Geochemistry, Guangzhou Institute of Geochemistry, Chinese Academy of Sciences, Guangzhou, China, [4]State Key Laboratory of Organic Geochemistry, Guangzhou Institute of Geochemistry, Chinese Academy of Sciences, Guangzhou, China, [5]Center of Deep Sea Research, Institute of Oceanology, Chinese Academy of Sciences, Qingdao, China, [6]Laboratory for Marine Mineral Resources, Qingdao National Laboratory for Marine Science and Technology, Qingdao, China, [7]CAS Center for Excellence in Tibetan Plateau Earth Sciences, Chinese Academy of Sciences, Beijing, China

Abstract Hydrothermal experiments were performed at 311°C and 3.0 kbar on natural olivine and peridotite to investigate the kinetics of serpentinization. The results show that the rates of reaction strongly depend on grain sizes of solid reactants, with smaller grain sizes resulting in faster kinetics. After 27 days of reaction, the reaction extent was 99% for peridotite with grain sizes of <30 μm, and the reaction extent was 28% for grain sizes of 100–177 μm. Compared to peridotite, olivine is serpentinized at much slower rates, e.g., 5.3% of reaction extent was achieved for olivine with grain sizes of 100–177 μm after 27 days, approximately five times lower than that reached during peridotite serpentinization. Such contrasting results are due to the presence of pyroxene and spinel, an interpretation which is supported by a marked increase in reaction extents for experiments with the addition of pyroxene and spinel. The reaction extent achieved in experiments with 3 wt % spinel greatly increased to 98% after 27 days, much higher than that achieved during olivine serpentinization. These results appear to be related to pyroxene and spinel releasing Al and Cr during serpentinization. As indicated by compositions of serpentine, orthopyroxene lost ~60% of Al at a reaction extent of 59%. Influence of Al and Cr is suggested by a dramatic increase in reaction extents with the addition of Al_2O_3 and Cr_2O_3 powders. Olivine in natural geological settings is commonly associated with pyroxene and spinel; consequently, serpentinization kinetics may be much faster than previously thought.

1. Introduction

Serpentinization, a low-temperature (<550°C) hydrothermal alteration of ultramafic rocks (typically peridotite and komatiite), has attracted considerable attention not only of geologists but also of chemists and biologists [e.g., *Charlou et al*., 1998, 2002; *Holm and Charlou*, 2001; *Kelley et al*., 2001; *Schrenk et al*., 2004, 2013; *Brazelton et al*., 2006, 2010; *Lang et al*., 2010; *Huang et al*., 2016]. Serpentinization primarily occurs in two geological settings on the Earth: (1) at spreading mid-ocean ridges where mantle-derived rocks react with seawater [e.g., *Hébert et al*., 1990; *Charlou et al*., 1998, 2002] and (2) in subduction zones via the reaction between peridotites from the mantle wedge and subduction-released aqueous fluids [e.g., *Hyndman and Peacock*, 2003; *Mével*, 2003]. The presence of serpentine has also been detected on the surface of Mars and other terrestrial planets [e.g., *Ehlmann et al*., 2008, 2009, 2010]. Serpentinization greatly modifies the physical, mechanical, and chemical properties of the oceanic lithosphere [e.g., *Scambelluri et al*., 1995; *Escartín et al*., 1997, 2001; *Guillot and Hattori*, 2013]. It leads to dramatic decreases in density and strength [*Escartín et al*., 1997, 2001] and possibly increases in volume [*Mével*, 2003]. A very low degree of serpentinization (~10%) significantly decreases the strength of olivine [*Escartín et al*., 1997, 2001]. Serpentine minerals can incorporate abundant H_2O (up to 13.5 wt %) and fluid-mobile elements, such as, Sr, and Ba [e.g., *Scambelluri et al*., 1995, 2001, 2004; *Hattori and Guillot*, 2003; *Deschamps et al*., 2012; *Guillot and Hattori*, 2013]. Thermodynamic and experimental simulations show that serpentine minerals can be stable at depths greater than 200 km [*Ulmer and Trommsdorff*, 1995; *Schmidt and Poli*, 1998]. This suggests that serpentinization delivers large quantities of H_2O and fluid-mobile elements into the mantle. In particular, serpentinization produces molecular hydrogen (H_2) and methane (CH_4) that can support communities of microorganisms [e.g., *Kelley et al*., 2001; *Schrenk et al*., 2004, 2013], which may be significant for the genesis of life in the early history of the Earth.

Despite extensive experimental investigation during the last 40 years [e.g., *Martin and Fyfe*, 1970; *Wegner and Ernst*, 1983; *Berndt et al*., 1996; *Jones et al*., 2010; *Malvoisin et al*., 2012ab; *Lafay et al*., 2012, 2014; *McCollom et al*., 2016], the mechanisms that control serpentinization processes, e.g., the kinetics of serpentinization, remain poorly understood. Serpentinization kinetics can greatly influence H_2 production [*Marcaillou et al*., 2011; *McCollom et al*., 2016], and they are essential parameters to quantify the proportions of serpentine and H_2O in subduction zones [e.g., *Allen and Seyfried*, 2004; *Emmanuel and Berkowitz*, 2006; *Iyer et al*., 2012]. Previous experiments on serpentinization kinetics have been performed mostly with olivine as the starting material [*Martin and Fyfe*, 1970; *Wegner and Ernst*, 1983; *McCollom and Bach*, 2009; *Malvoisin et al*., 2012ab; *Lafay et al*., 2012, 2014; *McCollom et al*., 2016]. The kinetics of olivine serpentinization strongly depend on temperature and compositions of starting fluids [*Martin and Fyfe*, 1970; *Wegner and Ernst*, 1983; *McCollom and Bach*, 2009; *Malvoisin et al*., 2012ab; *Lafay et al*., 2012, 2014; *McCollom et al*., 2016]. The reaction rates increase with increasing temperatures up to ~300°C, and they decrease significantly at temperatures of ≥350°C when olivine can exist in equilibrium with H_2O [*Martin and Fyfe*, 1970; *Wegner and Ernst*, 1983; *McCollom and Bach*, 2009; *Malvoisin et al*., 2012b]. Serpentinization proceeds at the highest speed in alkaline fluids, as compared to CO_2-rich and acidic fluids [*Lafay et al*., 2012, 2014].

Few experimental studies have addressed the kinetics of peridotite serpentinization directly [*Seyfried et al*., 2007; *Marcaillou et al*., 2011]. Although olivine is one of the most abundant minerals in peridotite, it may not necessarily act as a peridotite equivalent during serpentinization. Compared to peridotite, olivine serpentinization at ~300°C produces much less quantities of H_2 and CH_4 [*Huang et al*., 2015]. In contrast, olivine serpentinization may form larger amounts of iron oxide than those produced after peridotite serpentinization at the early stage of reactions, as pyroxene accommodates some iron from olivine during serpentinization [*Huang et al*., 2017]. These observations suggest that the process of olivine serpentinization may differ greatly from the process of peridotite serpentinization. Although it has been proposed that olivine and peridotite have similar serpentinization rates [*Malvoisin et al*., 2012b], the rates of olivine and peridotite serpentinization among previous studies were investigated under different experimental conditions, including compositions of starting fluids and calibration methods for quantifying serpentinization kinetics [*Seyfried et al*., 2007; *Marcaillou et al*., 2011; *Malvoisin et al*., 2012b]. This suggests that the comparison between the kinetics of olivine and peridotite serpentinization in previous studies may not be valid. The influence of pyroxene and spinel on serpentinization kinetics, however, has not been quantified, which may be significant in understanding the mechanisms of serpentinization processes.

In this study, we performed experiments at 311°C and 3.0 kbar using natural peridotite and olivine. The objectives are to (1) study the kinetics of olivine and peridotite serpentinization, (2) quantify the influence of pyroxene and spinel on serpentinization kinetics, and (3) illustrate the mechanisms that control serpentinization processes.

2. Materials and Methods

2.1. Preparation of Starting Materials

An unaltered peridotite composed of ~65 vol % olivine, 20 vol % orthopyroxene, 10–15 vol % clinopyroxene, and ~2 vol % spinel was used as a starting material. The peridotite was sampled at Panshishan (Jiangsu province, China) where it occurs as xenoliths in alkaline basalts [*Chen et al*., 1994; *Sun et al*., 1998; *Xu et al*., 2008]. The loss on ignition of the peridotite is very low, <0.5 wt % [*Yang*, 2008], which suggests that the sample is fresh. Compositions of primary minerals in this peridotite were determined by electron microprobe (Table S1 in the supporting information). More than 15 analyses were performed for each mineral, with relative error of <3%, suggesting that primary minerals are homogenous. The sample was crushed, ground in an agate mortar, and then sieved into starting grain sizes of <30, 86–105, 100–177, and 250 μm. These powders were then washed in an ultrasonic bath with pure water to remove very fine particles.

Olivine grains were picked from crushed peridotite (>250 μm) under a binocular microscope; those with inclusions of other minerals were excluded. The grains were washed in an ultrasonic bath with pure water to remove very fine particles. After drying at 60°C, olivine grains were ground in an agate mortar and sieved into starting grain sizes of <30 and 100–177 μm. Spinel grains were picked from the crushed peridotite (>250 μm) following the same procedure, and mechanical mixtures of olivine and spinel were prepared in order to study the influence of the presence of spinel on olivine serpentinization. In addition, mixtures of

Table 1. Experimental Conditions and Results[a]

Sample	Solid Reactants	Grain Sizes (μm)	*W/R* Ratios[b]	Time (Days)	Serpentine (wt%)[c]	Residual Olivine (wt%)	Residual Pyroxene (wt%)
HR106	olivine	<30	0.9	10	62(0.5)	38(0.5)	—
HR87	olivine	<30	0.71	14	67(3.4)	33(3.4)	—
HR76	olivine	<30	1.04	27	76(1.7)	25(1.7)	—
Fe37	olivine	100–177	1.1	27	5.3(1.0)	92(0.7)	—
HR105	peridotite	<30	1	10	92(2.4)	6.2(0.99)	0.0(0.99)
HR91	peridotite	<30	0.89	14	95(4.0)	4.8(2.1)	0.0(2.1)
HR86	peridotite	<30	0.86	27	99(1.7)	1.3(2.2)	0.0(2.2)
HR77	peridotite	100–177	1.2	28	24(1.7)	34(0.72)	36(0.72)
HR61	peridotite	100–177	0.82	123	59(3.3)	20(1.4)	16(1.4)
HR25	peridotite	86–105	1.4	19	31(1.6)	31(0.68)	32(0.68)
HR31	peridotite	250	1.1	20	16(3.6)	51(1.6)	28(1.6)
HR93	olivine + spinel (1.9 mg)	<30	0.93	27	99(0.9)	1.0(0.9)	—
HR75	olivine + spinel (6.6 mg)	<30	0.92	27	100(0.5)	0.0	—
HR92	olivine + Al_2O_3 (6.4 mg)	<30	0.82	27	90(0.7)	9.6(0.7)	—
HR95	olivine + Cr_2O_3 (6.3 mg)	<30	0.91	27	77(3.2)	23(3.2)	—
HR99	olivine + Cr_2O_3 (13.2 mg)	<30	0.9	27	84(2.8)	16(2.8)	—
HR88	spinel-free peridotite	<30	0.91	27	100	0.0	0.0

[a]The mass of olivine and peridotite loaded into gold capsules is ~50 mg for all experiments listed.
[b]Water/rock ratios: Ratios between mass of the starting fluid and solid reactants at start of experiments.
[c]Numbers in brackets are the standard deviation of at least 3 times analyses (±1δ).

olivine and pyroxene were prepared by removing spinel from crushed peridotite powders (<60 mesh) in order to study the influence of pyroxene on serpentinization reactions. The mixtures were washed in an ultrasonic bath with pure water to remove very fine particles. After drying at 60°C, these mixtures were ground in an agate mortar and then sieved into starting grain sizes of <30 μm. A saline solution (0.5 mol/L NaCl) was prepared with analytical-grade sodium chloride and deionized water.

2.2. Preparation of Gold Capsules

The solid reactants (~50 mg) and saline solution (~50 mg) were loaded into gold capsules (~30 mm long with a 4.0 mm outer diameter and a 0.2 mm wall thickness). Gold has been commonly used in serpentinization experiments because it is chemically inert and does not form any Fe-Au alloys under the investigated conditions [e.g., *Moody*, 1976; *Berndt et al.*, 1996; *Malvoisin et al.*, 2012b]. Gold capsules were sealed at both ends with a tungsten inert gas high-frequency pulse welder (PUK3) or an arc welder. Leaks were checked by placing the sealed capsules in a drying furnace at 100°C for at least 2 h. Only those capsules with mass differences less than 0.5% were used in the experiments.

2.3. Serpentinization Experiments

All experiments were conducted in cold-seal hydrothermal vessels at Guangzhou Institute of Geochemistry, Chinese Academy of Sciences (Table 1). The capsule was placed into the end of the hydrothermal vessels, followed by a filler rod (~6 cm long). Water was used as the pressure medium. Pressure was achieved by pumping water into the hydrothermal vessels and measured by a pressure gauge with a precision of ±100 bar. Temperature was monitored with an external K-type thermocouple that was inserted into a hole near the end of the vessel. The accuracy of temperature recording was within ±2°C. Quenching was facilitated with immersion in water, and temperatures decreased to <100°C within 10 s.

2.4. Scanning Electron Microscope

The surface morphology of solid products was characterized by a Zeiss Ultra 55 field emission scanning electron microscope at the Second Institute of Oceanography, State Oceanic Administration of China. Samples were dispersed onto a double-sided carbon tape and coated with a thin film of platinum for observation.

2.5. Fourier Transform Infrared Spectroscopy

The mineralogy of solid products was identified by Fourier transform infrared (FTIR) spectroscopy with a Bruker Vector 33 FTIR spectrometer at the Analytical and Testing Center of South China University of Technology. Infrared spectra were obtained at wave numbers ranging from 400 to 4000 cm^{-1} at a

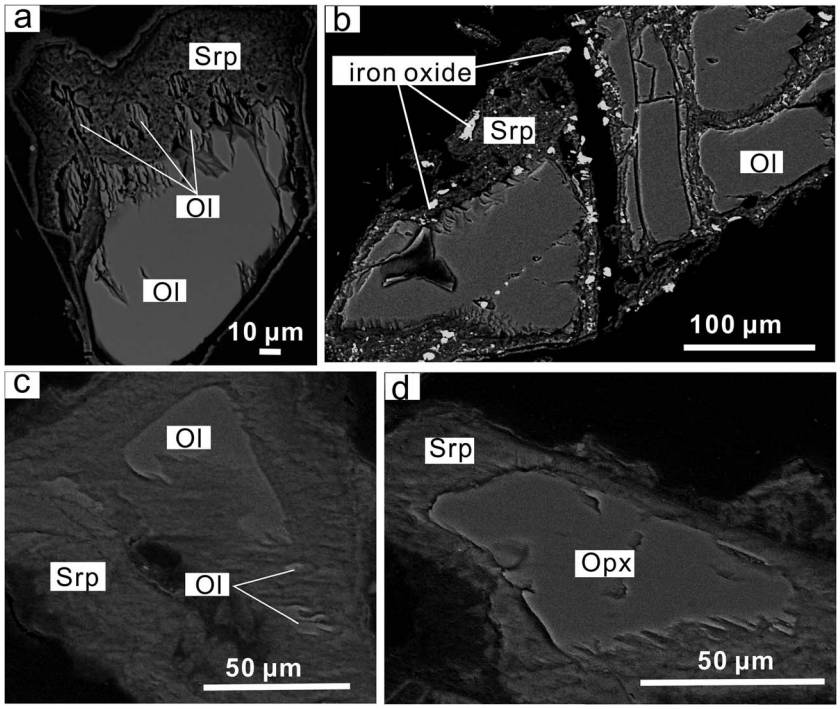

Figure 1. Backscattered electron images of the reaction products in experiments on peridotite and olivine. (a) HR77: olivine was replaced by serpentine, forming dissolution patterns and olivine subgrains. (b) Fe37: mesh-textured olivine was produced resulting from dissolution and cracking. (c) HR25: olivine subgrains still remained when olivine was extensively serpentinized. (d) HR25: dissolution features formed when orthopyroxene was replaced by serpentine minerals.

resolution of 4 cm^{-1}, and 32 scans were accumulated for each spectrum. The KBr pellets were prepared by mixing approximately 1 mg of sample powder with 200 mg of KBr.

2.6. Electron Microprobe

Compositions of residual olivine, pyroxene, and serpentine minerals were determined using a JEOL JXA 8100 electron microprobe at the Second Institute of Oceanography, State Oceanic Administration of China. Operating conditions of the electron beam were accelerating potential of 15 kV and beam current of 20 nA. A beam diameter of 15 μm was used for serpentine minerals to avoid devolatilization, whereas a beam diameter of 5 μm was used for olivine and pyroxene minerals. The calibration standards used were jadeite (Si and Na), olivine (Mg), almandine garnet (Fe and Al), diopside (Ca), sanidine (K), chromium oxide (Cr), rutile (Ti), nickel silicide (Ni), rhodonite (Mn), and tugtupite (Cl). The counting times for Ni, Co, Mn, Cr, and Cl were 30 s for peak and 10 s for background, whereas other elements were analyzed with 10 s for peak and 5 s for background.

3. Results and Discussion

3.1. Characterization of Experimental Products

Backscattered electron images of solid experimental products show that olivine and pyroxene were replaced by serpentine minerals, with or without the presence of iron oxide, leading to the formation of dissolution patterns and olivine subgrains (Figure 1). Serpentinized olivine typically has a mesh texture (Figure 1b) that has been reported in natural samples [e.g., *Bach et al*., 2006; *Beard et al*., 2009]. The formation of serpentine was attested by its typical infrared bands at 954 cm^{-1}, 1087 cm^{-1}, and 3686 cm^{-1} [e.g., *Fuchs et al*., 1998; *Lafay et al*., 2014]. The bands at 954 cm^{-1} and 1087 cm^{-1} correspond to the Si-O group of serpentine, and the band at 3686 cm^{-1} corresponds to the –OH group [e.g., *Fuchs et al*., 1998; *Lafay et al*., 2014]. Analyses of solid experimental products by electron microprobe also suggest that serpentine minerals are the main secondary hydrous minerals formed (Table S2). As suggested by scanning electron microscope imaging,

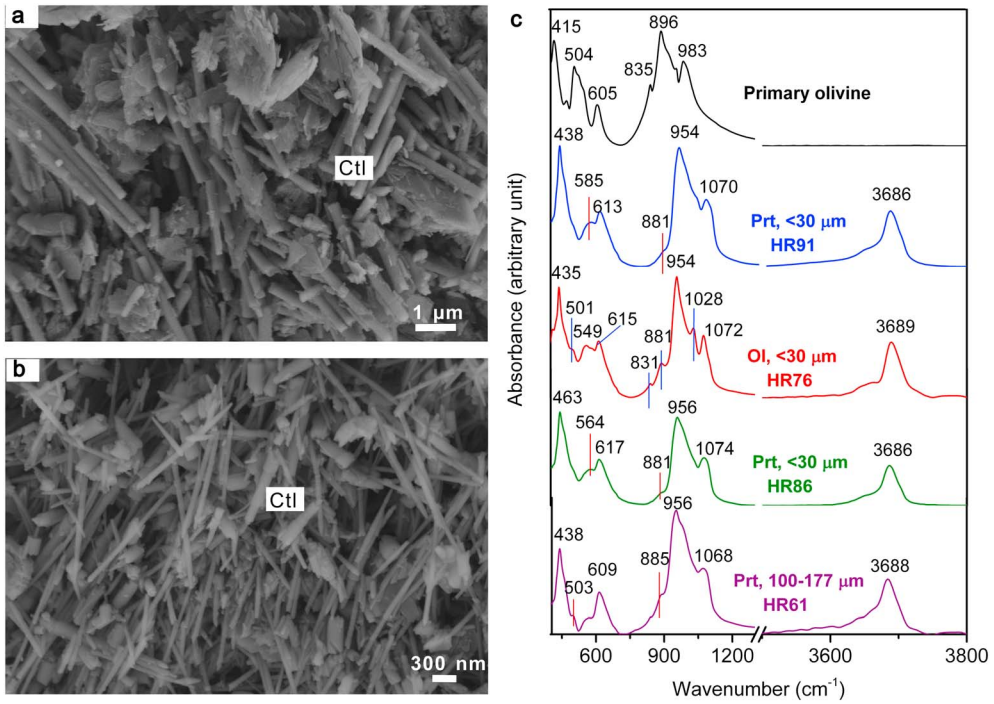

Figure 2. Identification of the experimental products using scanning electron microscopy imaging and Fourier transform infrared spectroscopy analyses. (a) HR61, peridotite with starting grain sizes of 100–177 μm. (b) HR76, olivine with starting grain sizes of <30 μm. Chrysotile (Ctl) fibers were produced. (c) FTIR spectra of the starting olivine and experimental products. Olivine has typical infrared modes at 504 cm^{-1}, 835 cm^{-1}, and 896 cm^{-1} [e.g., *Jeanloz*, 1980], and chrysotile is characterized by infrared bands at 610 cm^{-1}, 960 cm^{-1}, and 3689 cm^{-1} [e.g., *Fuchs et al.*, 1998; *Lafay et al.*, 2014]. Prt: Peridotite, Ol: olivine.

serpentine polymorphs are mainly composed of fibrous chrysotile (Figure 2). The diameter of chrysotile greatly depends on the starting grain sizes of olivine and peridotite (Figure 2). It increases from ~100 nm for starting grain sizes of <30 μm to ~300 nm for starting grain sizes of 100–177 μm.

Brucite was absent in all experimental products of this study. The formation of brucite can be strongly influenced by temperature, silica activity, and experimental duration [*Seyfried et al.*, 2007; *McCollom and Bach*, 2009; *Marcaillou et al.*, 2011]. Thermodynamic models suggest that the production of brucite decreases greatly at higher temperatures, and brucite is absent at ~350°C [*McCollom and Bach*, 2009]. Moreover, brucite is not stable at higher silica activity [*Bach et al.*, 2006; *Beard et al.*, 2009; *Marcaillou et al.*, 2011]. This may explain the absence of brucite in the experimental products after peridotite serpentinization, because peridotite has approximately one order of magnitude higher silica activity than olivine [*Allen and Seyfried*, 2003]. Besides temperature and silica activity, the production of brucite seems to depend on experimental duration [*Okamoto et al.*, 2011; *McCollom et al.*, 2016]. Hydrothermal experiments conducted at 300°C and 0.5 kbar on olivine serpentinization show that brucite was not formed after a short run duration (~75 days), whereas it was produced after a longer reaction period [*McCollom et al.*, 2016].

3.2. Determination of Serpentinization Rates

The serpentinization kinetics in the experiments of this study were quantified by FTIR. Infrared spectroscopy is very sensitive to the presence of serpentine, at levels as low as ~0.1 wt % [e.g., *Foresti et al.*, 2003]. This technique has already been used to determine the percentage of serpentine in soils and in the experimental products after serpentinization of olivine [e.g., *Foresti et al.*, 2003; *Lafay et al.*, 2012, 2014]. In order to quantify the proportions of serpentine, the only hydrous mineral produced in experimental products of this study, we established two standard curves according to infrared spectra of mechanical mixtures of serpentine and olivine or peridotite. A standard curve based on mixtures of serpentine and peridotite was used to calibrate the proportions of serpentine in experiments with peridotite (Figure 3a), and a standard curve based on mixtures of serpentine and olivine was used to quantify the proportions of serpentine in

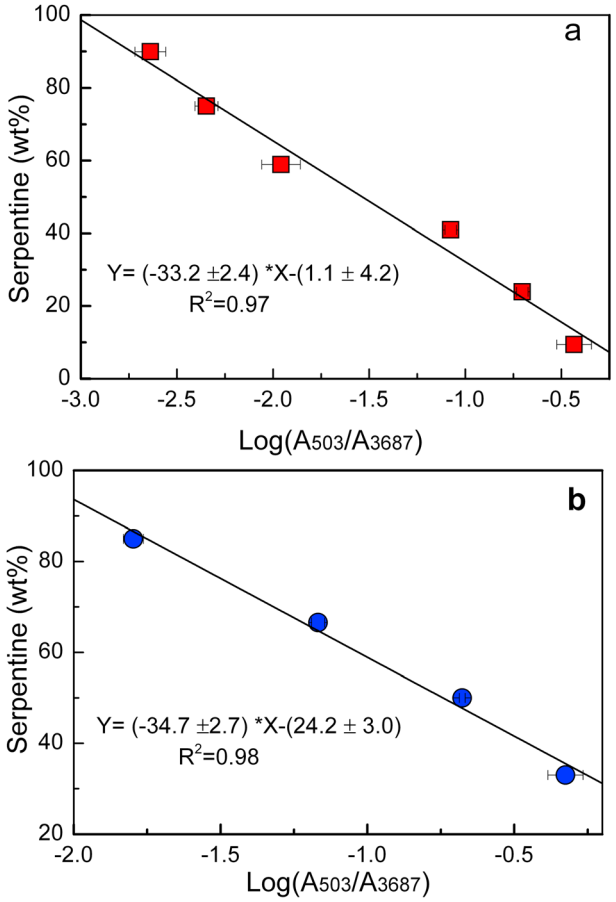

Figure 3. Standard curves used to calibrate the proportions of serpentine in the experiments of this study on (a) peridotite and (b) olivine.

experiments with olivine (Figure 3b). The percentage of serpentine is negatively correlated with the integrated intensity ratios $\log(A_{503}/A_{3687})$ (Figure 3), where A_{503} corresponds to the integrated intensity of the Si-O group in olivine at wave numbers ranging from 484 to 522 cm^{-1} and A_{3687} is the integrated intensity of the –OH group in serpentine at wave numbers from 3612 to 3745 cm^{-1}. The baseline correction and integrated intensities were obtained by Origin 8.6 following the same procedures for all analyzed samples. The advantage of using intensity ratios for calibration is that it can minimize weight uncertainties. Analyses with varied amounts of solid products yield essentially the same results. Repeated measurements (>3 times) suggest that the precision is within ±4%.

Reaction extents (%) are illustrated in Figure 4 as a function of reaction time (days). The serpentinization kinetics greatly depend on starting grain sizes of olivine and peridotite, with smaller grain sizes resulting in faster rates (Figure 4). After 27 days of reaction, the reaction extent was 99% for peridotite with starting grain sizes of <30 μm, and the reaction extent was 28% for peridotite with starting grain sizes of 100–177 μm (Table 1). Compared to peridotite, olivine had much slower rates of serpentinization (Figure 4). The reaction extent was 5.3% for olivine with starting grain sizes of 100–177 μm after 27 days, approximately five times lower than the reaction extent reached in experiments on peridotite over the same period (Figure 4 and Table 1). The contrast therefore appears to result from the presence of spinel and pyroxene in peridotite.

3.3. Influence of Pyroxene and Spinel on Serpentinization Kinetics

Hydrothermal experiments were performed at 311°C and 3.0 kbar with mechanical mixtures of olivine and spinel or pyroxene as starting materials in order to study the influence of pyroxene and spinel on serpentinization kinetics (Table 1). As shown in Figure 5, the presence of pyroxene and spinel greatly accelerated the rates of olivine serpentinization. After 27 days of reaction, 76% of reaction extent was reached in olivine-only experiments, and this increased greatly to 98% with the presence of 3% spinel. Complete serpentinization was reached after 27 days in the presence of pyroxene (Figure 5 and Table 1). These observations suggest that pyroxene and spinel promote the olivine serpentinization reactions.

Previous hydrothermal experiments show that orthopyroxene and clinopyroxene are more resistant to serpentinization than olivine at ~300°C [*Marcaillou et al*., 2011]. For abyssal peridotite with a reaction extent of 60%–90%, olivine is completely replaced by serpentine, whereas clinopyroxene and spinel remain fresh [e.g., *Seyler et al*., 2003]. Therefore, it would be expected that peridotite should have slightly slower serpentinization rates compared to olivine if a chemical interaction does not exist between olivine and pyroxene or spinel during serpentinization. However, the experimental results of this study show that peridotite is serpentinized at a much higher rate than olivine alone (Figure 4), indicating a chemical interaction between olivine and pyroxene or spinel occurred during serpentinization.

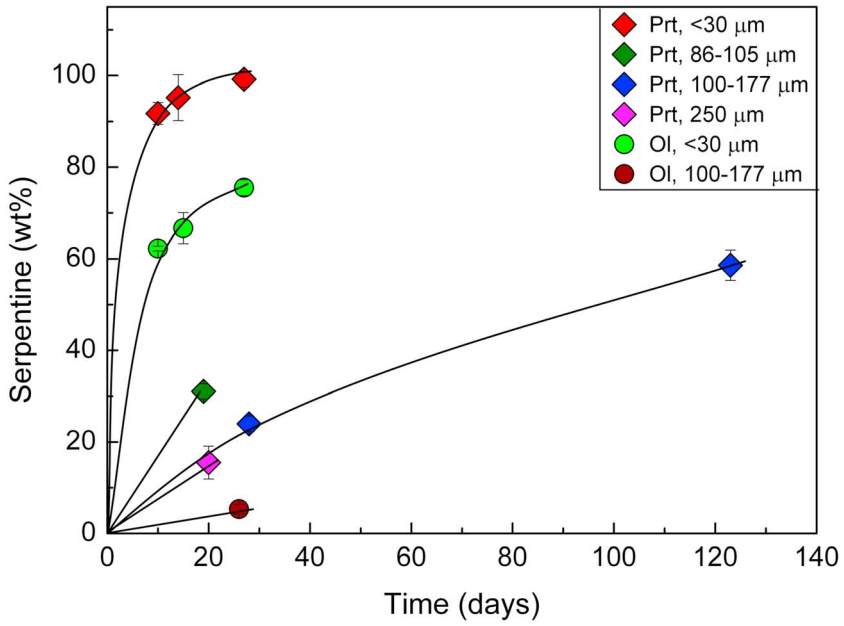

Figure 4. Serpentinization degree (%) as a function of time (days) for experiments on peridotite (filled diamond) and olivine (filled circle), showing that peridotite has much faster rates of serpentinization than olivine. Data were fitted using a kinetic pseudo second-order model.

Chemical compositions of serpentine minerals indicate release of Al and Cr from pyroxene during serpentinization (Figure 6). For experiments of this study on peridotite with starting grain sizes of 100–177 μm, orthopyroxene-derived serpentine formed after 20 days had 3.4 ± 0.6 wt % Al_2O_3, which decreased significantly to 1.7 ± 0.2 wt % after 120 days (Figure 6), much lower than the Al_2O_3 content of the primary orthopyroxene (4.1 ± 0.2 wt %). This suggests that orthopyroxene released ~20% of its Al at a reaction extent of 31% and 60% Al at a reaction extent of 59%. In contrast, olivine-derived serpentine had a higher

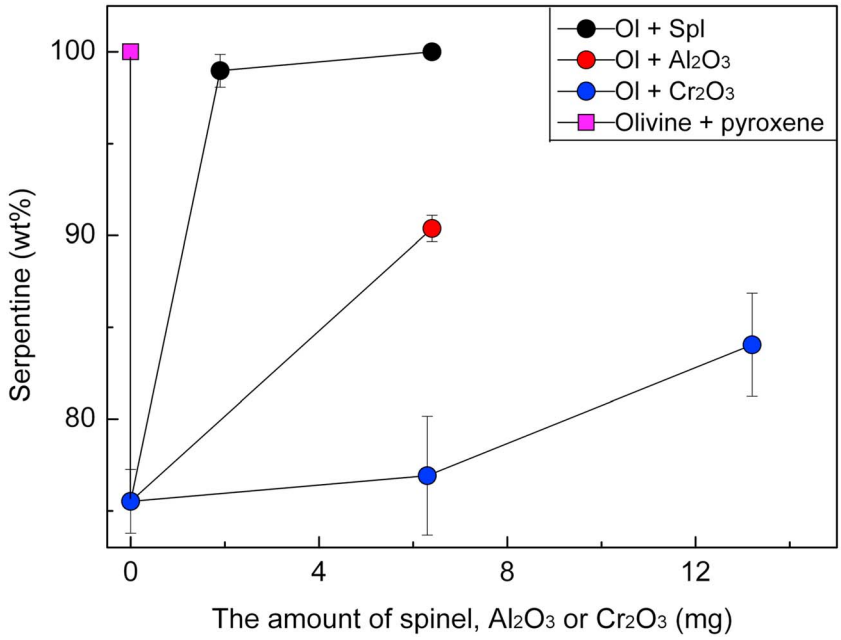

Figure 5. Influence of pyroxene, spinel, Al_2O_3, and Cr_2O_3 on serpentinization kinetics. All the data listed correspond to experiments with run duration of 27 days. The presence of pyroxene, spinel, Al_2O_3, and Cr_2O_3 significantly promote olivine serpentinization.

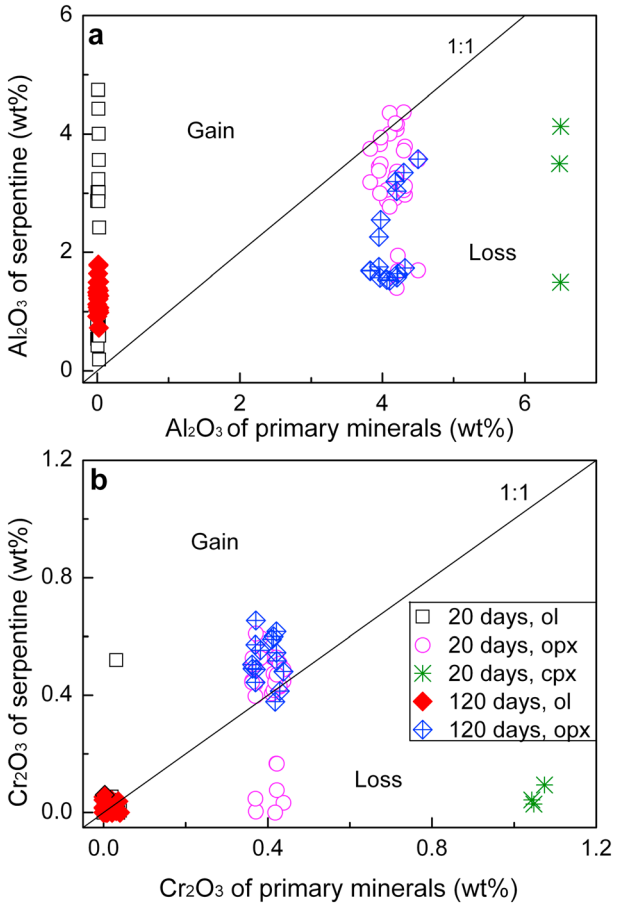

Figure 6. Partitioning of (a) Al_2O_3 and (b) Cr_2O_3 between primary minerals (olivine, orthopyroxene, and clinopyroxene) and their coexisting serpentine in experiments with peridotite. The data above the 1:1 line indicate a gain of aluminum and chromium during serpentinization, and the data below the 1:1 line suggest a loss of aluminum and chromium. Ol: olivine; Opx: orthopyroxene; Cpx: clinopyroxene.

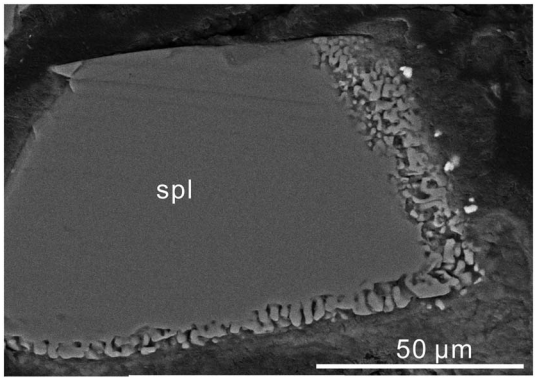

Figure 7. Representative backscattered electron imaging of spinel in the experimental products of this study. Spinel (spl) was hydrothermally altered resulting in the formation of dissolution grains at the edge.

Al_2O_3 content than that of primary olivine (0.01 ± 0.01 wt % Al_2O_3). For experiments on peridotite with starting grain sizes of 100–177 μm, olivine-derived serpentine had 1.9 ± 1.3 wt % Al_2O_3 after 20 days, and this became more homogenous after 120 days, 1.3 ± 0.1 wt % (Figure 6), suggesting that olivine accommodated Al released from orthopyroxene during serpentinization. Consistently, analyses of natural serpentinites show that orthopyroxene lost ~50% of its Al to olivine during serpentinization [e.g., *Dungan*, 1979; *Golightly and Arancibia*, 1979; *Hébert et al*., 1990]. On the other hand, orthopyroxene-derived serpentine had Cr_2O_3 contents ranging from ~0.1 wt % to ~0.6 wt %, which are lower or higher than the Cr_2O_3 contents of the primary orthopyroxene (0.40 ± 0.03 wt %, Figure 6b). In contrast, clinopyroxene-derived serpentine contained Cr_2O_3 contents much lower than those of the clinopyroxene hosts. Therefore, pyroxene minerals, and especially clinopyroxene, lost some Cr during serpentinization, which is consistent with observations of natural samples [e.g., *Hébert et al*., 1990].

Spinel in natural serpentinites is commonly associated with coatings and rinds of magnetite derived from serpentinization of olivine [e.g., *Beeson and Jackson*, 1969; *Hamlyn*, 1975; *Burkhard*, 1993; *Mellini et al*., 2005]. Typical features of spinel in the experimental products of this study were observed by backscattered electron imaging, and spinel was hydrothermally altered forming dissolution grains (Figure 7). These grains are much brighter than primary spinel (Figure 7). Chemical compositions of the dissolution grains were analyzed with electron microprobe, and it shows that they have a significantly lower Al_2O_3 content (~30 wt %) but a slightly lower Cr_2O_3 content (~12 wt %) compared to primary spinel (56 wt % Al_2O_3 and 12.8 wt % Cr_2O_3). This suggests that Al and Cr were released from spinel during serpentinization.

In order to quantitively study the influence of Al and Cr on serpentinization

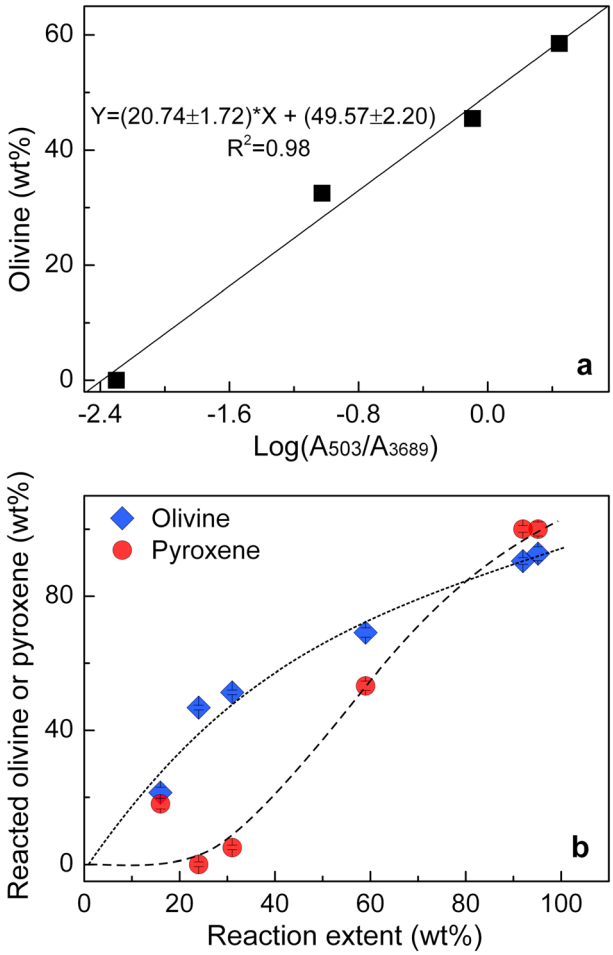

Figure 8. (a) A standard curve used to quantify the proportions of residual olivine in the experimental products of this study. (b) The proportion of serpentinized olivine or pyroxene (wt %) as a function of the extent of reaction, showing that serpentine minerals are predominantly derived from olivine serpentinization at the early stage of serpentinization (reaction extents of <50%).The proportion of serpentinized olivine is the mass ratio between olivine that experienced serpentinization and primary olivine.

kinetics, we performed experiments at 311°C and 3.0 kbar with mechanical mixtures of olivine and Al_2O_3 or Cr_2O_3 powders as starting materials (Table 1). As shown in Figure 5, Al and Cr accelerated the kinetics of olivine serpentinization. After 27 days of reaction, the reaction extent was 90% with the presence of 11 wt % Al_2O_3, much higher than the reaction extent reached in the olivine-only experiments (76%, Table 1). Despite this increase, serpentinization kinetics are slower compared to those in experiments with the presence of pyroxene and spinel (Figure 5). This suggests that the faster rates of peridotite serpentinization arise from the joint influence of Al and Cr. On the other hand, pyroxene minerals have more abundant SiO_2 than olivine. Hydrothermal experiments show that pyroxene serpentinization releases SiO_2 around one order of magnitude higher compared to the SiO_2 leached during olivine serpentinization [*Allen and Seyfried*, 2003]. When the experimental duration was increased from 20 to 120 days, the SiO_2 content of orthopyroxene-derived serpentine decreased greatly, whereas the SiO_2 content of olivine-derived serpentine increased [*Huang et al.*, 2017], indicating the release of silica from orthopyroxene during serpentinization. The influence of silica on serpentinization kinetics, however, may be negligible, supported by comparable reaction extents achieved in experiments with mechanical mixtures of olivine and pyroxene or spinel. Otherwise, the kinetics of serpentinization in experiments with the presence of pyroxene should be much faster than that with the addition of spinel.

To illustrate the release of Al and Cr from pyroxene and spinel during peridotite serpentinization, we quantified the proportion of serpentinized olivine in the experiments of this study, i.e., the mass ratio between olivine that was replaced by serpentine and primary olivine. The amount of residual olivine in the experimental products was calibrated according to a standard curve based on infrared spectra of mechanical mixtures of peridotite and serpentine (Figure 8a). It shows that the amount of olivine in the mixtures is positively correlated with the integrated intensity ratios $\log(A_{503}/A_{3689})$ (R^2 = 0.98, Figure 8a). The amount of residual pyroxene in the experimental products was obtained based on mass balance. Consequently, the proportion of serpentinized pyroxene, i.e., the mass ratio between pyroxene that was replaced by serpentine and primary pyroxene, was determined. The percentage of serpentinized olivine or pyroxene is shown in Figure 8b versus reaction progress. It shows that serpentine minerals were predominantly derived from olivine serpentinization at a reaction extent of <~50%, and they were formed from serpentinization of olivine and pyroxene as the reaction proceeds (Figure 8b). Consistently, observations of natural samples show that olivine hydration is the main serpentine-forming process at the early stage of peridotite serpentinization [*Bach et al.*, 2006;

Seyfried et al., 2007; *Beard et al*., 2009; *Marcaillou et al*., 2011]. It implies that pyroxene released most of the Al at a reaction extent of >50%.

The mechanism whereby Al promotes olivine serpentinization is possibly due to the formation of Al-Si complexes. Hydrothermal experiments have shown that the solubility of Al in pure water is very low, whereas it becomes five times higher in the presence of silicate minerals, such as kyanite and quartz, arising from complexing between Al and Si [*Salvi et al*., 1998; *Manning*, 2007]. These studies also observed that the formation of Al-Si complexes greatly increases the solubility of silicate minerals [*Salvi et al*., 1998; *Manning*, 2007]. Therefore, Al released by pyroxene and spinel in the experiments of this study may be complexed with the Si leached by dissolving olivine and pyroxene, which may increase the rates of olivine dissolution. For the experiments of this study, typical dissolution features formed not only at the early stage of serpentinization (Figure 1b), but they also occurred when primary olivine was mostly replaced by serpentine (Figure 1c). Dissolution features were also observed in previous experimental products [*Malvoisin et al*., 2012b; *Lafay et al*., 2012, 2014] and in natural samples [e.g., *Liu et al*., 2010]. This suggests that serpentinization processes are commonly associated with dissolution features that have been proposed to be the rate-limiting process during serpentinization [*Lafay et al*., 2012, 2014; *Malvoisin et al*., 2012b]. This further suggests that the influence of Al on serpentinization kinetics is attributed to an increase in the rates of olivine dissolution.

Chromium accelerates the rates of olivine serpentinization, possibly because of the release of water-soluble Cr^{6+} from spinel and Cr_2O_3. Hexavalent chromium oxidizes Fe^{2+} derived from olivine and pyroxene into Fe^{3+} (reaction (1)), which may result in the formation of secondary Fe^{3+}-bearing minerals, e.g., magnetite and serpentine.

$$Cr^{6+} + 3Fe^{2+} \rightarrow 3Fe^{3+} + Cr^{3+} \quad (1)$$

Analyses of natural samples and experimental products show that serpentine minerals can incorporate up to 90% Fe^{3+} [*Seyfried et al*., 2007; *Marcaillou et al*., 2011; *Evans et al*., 2013]. The production of Fe^{3+} also arises from olivine serpentinization, which accompanies the formation of H_2 (reaction (2)):

$$2Fe^{2+} + 2H_2O = 2Fe^{3+} + H_2 + 2OH^- \quad (2)$$

As a consequence, serpentinization may take place at a very low oxygen fugacity, i.e., the oxidation-reduction paradox of serpentinization [*Evans et al*., 2013]. Olivine serpentinization at 300°C and 0.5 kbar produced 158 mmol/kg H_2 after 69 days, with an oxygen fugacity ~6 log units below Faylite-magnetite-quartz (FMQ) buffer [*Berndt et al*., 1996]. For experiments of this study on peridotite with starting grain sizes of <30 μm, 167 mmol/kg H_2 was produced after 14 days [*Huang et al*., 2015]. This agreement in H_2 release suggests that the oxygen fugacity of this study is very low. As a consequence, Cr^{6+} released from spinel may be reduced directly to Cr^{3+} via its reaction with H_2, as evidenced by the formation of fine Cr_2O_3 grains in the experimental products. The involvement of Cr^{6+} in serpentinization has also been supported by previous experimental results and analyses of natural samples [*Ulmer*, 1974; *Farkaš et al*., 2013]. Aqueous fluids equilibrated with spinel at 25°C have ~5–10 ppm Cr^{6+} [e.g., *Ulmer*, 1974]. This may lead to the formation of Cr-depleted ferrichromite and magnetite rinds as observed in natural serpentinites [e.g., *Ulmer*, 1974; *Burkhard*, 1993; *Mellini et al*., 2005]. Moreover, naturally serpentinized peridotite has much heavier chromium isotope compositions ($\delta^{53}Cr/^{52}Cr$) compared to primary peridotite [*Farkaš et al*., 2013]. In particular, $\delta^{53}Cr/^{52}Cr$ of serpentinized peridotite increases with progressive serpentinization, indicating the involvement of Cr^{6+} during serpentinization because Cr^{6+} has heavier $\delta^{53}Cr/^{52}Cr$ than Cr^{3+} [*Farkaš et al*., 2013]. Hexavalent Cr can oxidize Fe^{2+} derived from olivine and pyroxene into Fe^{3+} (reaction (1)), which may induce the reaction of olivine dissolution to the right side (reaction (3)), possibly resulting in an increase in the rates of olivine serpentinization.

$$(Mg_{0.9}, Fe_{0.1})SiO_4 = 0.9Mg^{2+} + 0.1Fe^{2+} + {SiO_4}^{2-} \quad (3)$$

3.4. The Kinetic Pseudo Second-Order Model

A kinetic pseudo second-order model was used to fit the experimental data of this study. This model has been commonly used to describe the sorption of pollutants from aqueous solutions, the crystal growth of

Table 2. Kinetic Parameters Obtained From the Pseudo Second-Order Model

Solid Reactant	Starting Grain Size (μm)	ξ_{max}(%) Exp.	ξ_{max}(%) Calc.	$t_{1/2}$ (Days)	Initial Rate(1/s)	Fitting r^2
Olivine	<30	76	100	7.1 ± 1.9	1.61E−06 ± 2.74E−07	0.992
Olivine	100–177	5.3	100	431 ± 374	2.69E−08 ± 2.33E−08	0.990
Peridotite	<30	99	100	0.8 ± 0.4	1.96E−05 ± 2.05E−05	0.999
Peridotite	100–177	59	100	87.5 ± 2.7	1.32E−07 ± 4.11E−09	0.999
Peridotite	250	15	100	109 ± 0.3	1.06E−07 ± 2.91E−09	0.999

calcite, and serpentinization processes [e.g., *Ho and McKay*, 1999; *Montes-Hernandez et al*., 2009; *Lafay et al*., 2012, 2014]. The differential form of the kinetic model is

$$\frac{d\xi}{dt} = k(\xi_{max} - \xi)^2 \quad (4)$$

where k is the rate constant, ξ_{max} is the maximum alteration extent at apparent equilibrium (%), and ξ is the alteration extent (%) at time t (day). The integral form of equation (4) together with the boundary condition $t = 0$ and $\xi = 0$ produces a correlation between the alteration extent (ξ) and time (t):

$$\xi = \frac{\xi_{max} * t}{t1/2 + t} \quad (5)$$

A new parameter is defined ($t_{1/2} = 1/(k * \xi_{max})$), which represents the time after which half of the maximum alteration extent was achieved. The serpentinization initial rate is described as $v_0 = \xi_{max}/t_{1/2}$.

The initial rate of serpentinization greatly depends on the starting grain sizes of olivine and peridotite, with smaller grain sizes resulting in faster rates (Table 2). The serpentinization initial rate was 1.6×10^{-6} s^{-1} for olivine with starting grain sizes of <30 μm, whereas it significantly decreased to 2.7×10^{-8} s^{-1} for larger grain sizes (100–177 μm). Compared to olivine, peridotite has a much faster initial rate of serpentinization. The serpentinization initial rate for peridotite with starting grain sizes of <30 μm was 2.0×10^{-5} s^{-1}, around one order of magnitude faster than the serpentinization initial rate of olivine with the same grain size.

3.5. Comparison to Previous Results

Previous experiments on serpentinization kinetics were performed primarily on olivine [*Martin and Fyfe*, 1970; *Wegner and Ernst*, 1983; *Malvoisin et al*., 2012b; *Lafay et al*., 2012, 2014; *McCollom et al*., 2016]. The rates that have been reported to date are largely scattered (Figure 9). Serpentinization experiments of *Martin and Fyfe* [1970] and *Wegner and Ernst* [1983] were carried out with synthetic forsterite as the starting material. The serpentinization rates in these studies are relatively rapid. As reported by *Wegner and Ernst* [1983], 40% of reaction extent was achieved within 26 days for forsterite with starting grain sizes of 105–149 μm at 300°C and 3.0 kbar. In contrast, serpentinization kinetics for natural olivine with similar grain sizes are around one to two orders of magnitude slower [*Malvoisin et al*., 2012b; *McCollom et al*., 2016]. For natural olivine with starting grain sizes of 100–150 μm, <1% of reaction extent was reached within 141 days [*Malvoisin et al*., 2012b]. Our experimental results are consistent with this finding, with 5.3% of reaction extent being reached after 27 days for natural olivine with starting grain sizes of 100–177 μm (Figure 9 and Table 1).

A few experimental studies have examined the rates of peridotite serpentinization [*Seyfried et al*., 2007; *Marcaillou et al*., 2011]. Although it has been proposed that olivine and peridotite have similar serpentinization kinetics [*Marcaillou et al*., 2011; *Malvoisin et al*., 2012b], the rates of olivine and peridotite serpentinization among previous studies were investigated under different experimental conditions, including compositions of starting fluids, and calibration methods for quantifying serpentinization kinetics [*Seyfried et al*., 2007; *Marcaillou et al*., 2011; *Malvoisin et al*., 2012b]. Most experiments of *Malvoisin et al*. [2012b] were conducted at 300°C and 0.5 kbar with pure water, and reaction progress was determined mainly according to magnetic susceptibility of experimental products, which has a linear positive correlation with the proportions of serpentine [*Malvoisin et al*., 2012a]. The serpentinization rates reported by *Malvoisin et al*. [2012b], however, are largely scattered, e.g., for olivine with grain sizes of 5–15 μm, the reaction extent ranges from 30% to 89% after the same experimental duration (~75 days, Figure 9) [*Malvoisin et al*., 2012b].

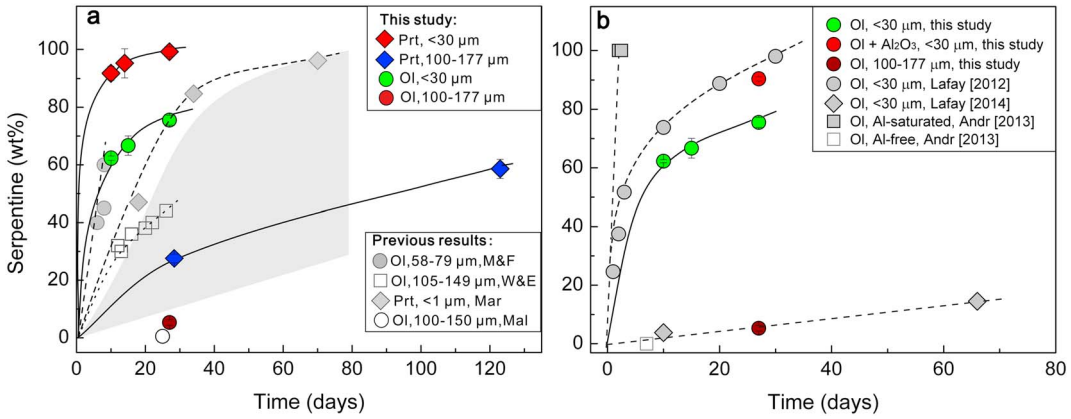

Figure 9. (a) Comparison of serpentinization kinetics from this study with data from previous experiments taking neutral starting fluids. Synthetic forsterite with grain sizes of 58–79 μm is from *Martin and Fyfe* [1970] (M&F), and synthetic forsterite with grain sizes of 105–149 μm is from experiments of *Wegner and Ernst* [1983] (W&E) at 270°C and 3.0 kbar. Natural peridotite with grain sizes of <1 μm is from *Marcaillou et al.* [2011] (Mar). Natural olivine with grain sizes of 100–150 μm is from *Malvoisin et al.* [2012b] (Mal). Gray area refers to the kinetic data from *Malvoisin et al.* [2012b] on olivine with grain sizes of 5–15 μm. (b) Influence of fluid compositions on the rates of olivine serpentinization. *Lafay et al.* [2012] (Lafay [2012]) refers to experiments with alkaline starting fluids, and *Lafay et al.* [2014] (*Lafay* [2014]) represents experiments with acidic or CO_2-saturated starting fluids. Experiments of *Andreani et al.* [2013] (*Andr* [2013]) were conducted at 300°C and 2.0 kbar in Al-supersaturated or Al-free starting fluids.

Magnetic susceptibility greatly depends on the crystal shape and grain size distribution of magnetite [e.g., *Fukuma and Dunlop*, 2006; *Smirnov*, 2009; *Ge and Liu*, 2014]. As suggested by an experimental simulation, magnetic susceptibility decreases by around one order of magnitude when grain sizes of magnetite increase from ~0.1 to 10 μm [*Smirnov*, 2009]. Magnetite that formed at very early stages of serpentinization can be dissolved and reprecipitated [*Malvoisin et al.*, 2012a; *Huang et al.*, 2017], producing magnetite with highly variable grain sizes. Magnetite produced in the experiments of *Malvoisin et al.* [2012b] has grain sizes ranging from <1 to 20 μm, possibly resulting in great uncertainties of serpentinization kinetics based on magnetic susceptibility.

The experiments of *Seyfried et al.* [2007] were performed with artificial seawater that contained abundant sulfate and bicarbonate salts, resulting in starting fluids relatively rich in CO_2. As indicated by hydrothermal experiments, H_2 and CH_4 production during serpentinization of olivine decrease with increasing CO_2 in the starting fluids [*Jones et al.*, 2010], which may influence the rates of olivine serpentinization. Moreover, the serpentinization kinetics in *Seyfried et al.* [2007] were quantified by numerical models, which may strongly depend on the parameters used. In particular, different serpentine polymorphs were produced in previous experimental studies [*Seyfried et al.*, 2007; *Marcaillou et al.*, 2011; *Malvoisin et al.*, 2012b], which may influence the rates of serpentinization. Lizardite is the major secondary hydrous mineral in the experiments of *Marcaillou et al.* [2011], whereas chrysotile is produced in *Seyfried et al.* [2007] and also in *Malvoisin et al.* [2012b] for olivine with starting grain sizes of <5 μm. As indicated by hydrothermal experiments, chrysotile formation requires a higher degree of solution supersaturation than lizardite production [*Normand et al.*, 2002], possibly leading to different inferred rates of olivine serpentinization.

In contrast, the experiments of this study were conducted under similar conditions. Chrysotile was produced after serpentinization of olivine and peridotite, and the reaction extent was quantified by infrared spectroscopy. In particular, different standard curves were established for experiments on olivine and peridotite in order to eliminate the matrix effect. The experimental results of this study clearly show that peridotite has much faster rates of serpentinization than olivine alone, resulting from the presence of pyroxene and spinel. This suggests that serpentinization kinetics can be strongly influenced by Al and Cr contents of fluids.

The influence of Al contents of starting fluids on serpentinization kinetics has also been investigated by *Andreani et al.* [2013]. They showed that Al increases the rates of olivine serpentinization by around one order of magnitude, and complete reactions for olivine chips (~100 μm wide) were achieved within two days (Figure 9b). The serpentinization kinetics of this study are slower than those reported by

Andreani et al. [2013], e.g., with the addition of 11% powdered Al_2O_3, complete serpentinization was not achieved for olivine with starting grain sizes of <30 μm after 27 days. The contrast may arise from higher supply of Al in *Andreani et al*. [2013], which can lead to faster serpentinization kinetics. Besides aluminum, serpentinization kinetics greatly depend on the pH of starting fluids [*Lafay et al*., 2012, 2014]. The serpentinization of olivine proceeds at the fastest speed in experiments with alkaline fluids, which is followed progressively by neutral and acidic fluids [*Lafay et al*., 2012, 2014; *Malvoisin et al*., 2012b]. For the experiments of this study, pH of the starting saline fluid is ~6.5. Therefore, the serpentinization rates in this study are slower than serpentinization kinetics in experiments with alkaline starting fluids [*Lafay et al*., 2012], and they are faster than the serpentinization kinetics in experiments with acidic starting fluids [*Lafay et al*., 2014].

3.6. Geological Implications

In natural geological settings, serpentinization kinetics greatly depend on the supply of Al and Cr from its neighboring Al, Cr-rich minerals. Aluminum is always present in serpentinites with Al_2O_3 contents ranging from <1 wt % to >20 wt % [e.g., *Dungan*, 1979; *Beard et al*., 2009]. Olivine in natural geological settings is typically closely associated with Al suppliers such as pyroxene, plagioclase, and amphibole. Aluminum is mobile during serpentinization processes where pyroxene and spinel can release some of their Al, forming Al-rich serpentine after olivine serpentinization (Figure 6). The mobility of Al in metamorphism and metasomatism is also indicated by occurrences of Al-rich minerals (such as kyanite) in veins [e.g., *McLelland et al*., 2002; *Sepahi et al*., 2004]. This suggests that Al can be actively involved in serpentinization processes. Chromium occurs primarily in the form of chromium-rich spinel that is a common accessory mineral in peridotite and serpentinite. Chromium may substitute for major elements (e.g., Al and Fe^{3+}) in silicate minerals such as pyroxene and amphibole. As reported by *Klein-BenDavid et al*. [2009], fluid inclusions in diamonds contain up to 1 wt % Cr_2O_3. Experiments show that the solubility of Cr_2O_3 increases greatly with increasing temperatures and pressures and that it can be significantly enhanced by salinity [*Klein-BenDavid et al*., 2011]. Therefore, chromium may be an important component of aqueous fluids in geological settings associated with serpentinization. Consequently, the kinetics of olivine serpentinization can be greatly enhanced.

Aluminum and chromium may therefore influence the formation of molecular hydrogen and methane during serpentinization. The effect of Al on H_2 production in natural geological settings has been described by *Seyfried et al*. [2011], and they showed that larger quantities of H_2 were detected in the presence of Al-bearing minerals such as plagioclase. Consistently, hydrothermal experiments suggest that peridotite serpentinization produces much larger quantities of H_2 and CH_4 compared to olivine serpentinization [*Huang et al*., 2015], likely because of the release of Al and Cr from pyroxene and spinel. Chromium can effectively catalyze the production of hydrocarbons, e.g., methane, ethane, and propane [e.g., *Foustoukos and Seyfried*, 2004]. This may be significant for the genesis of life in the early history of the Earth. Serpentinite-hosted hydrothermal fields commonly contain abundant H_2 and CH_4 that can support communities of microorganisms [e.g., *Kelley et al*., 2001; *Schrenk et al*., 2004, 2013]. The microorganisms can endure relatively high temperature (~100°C) and pressure. Biological studies have shown that the ultimate ancestor of life is a hyperthermophile, i.e., an organism that lives at, or possibly above, temperature of 80–110°C [e.g., *Sleep*, 2010]. As suggested by geological evidence, life has been present on the Earth for at least 3.5 Gyr and possibly occurred before 3.8 Gyr when ultramafic rocks may have been extensively exposed on the surface of the Earth [e.g., *Nisbet and Fowler*, 1996; *Zahnle et al*., 2007; *Sleep*, 2010]. The interaction between ultramafic rocks and H_2O in the early atmosphere may have initiated the prebiotic chemical conditions for the origin of life.

4. Conclusions

The rates of olivine and peridotite serpentinization were investigated experimentally at 311°C and 3.0 kbar. Compared to olivine, peridotite has much faster rates of serpentinization, e.g., the reaction extent for olivine with starting grain sizes of 100–177 μm was 5.3% after 27 days, whereas it increased by approximately five times over the same period for peridotite with similar starting grain sizes. The contrasting results arise from the presence of pyroxene and spinel releasing Al and Cr during serpentinization. The experiments of this study strongly suggest that pyroxene and spinel are important Al suppliers, e.g., orthopyroxene lost ~60%

of its Al to olivine at a reaction extent of 59%. Aluminum and Cr actively enhance olivine serpentinization, which is supported by experiments with the addition of Al_2O_3 and Cr_2O_3 fine powders. Our experiments also suggest that Al and Cr are mobile during serpentinization, which agrees well with previous experimental results [e.g., *Manning*, 2007; *Klein-BenDavid et al*., 2009, 2011] and occurrences of Al-rich minerals (e.g., kyanite) in veins during metamorphism and metasomatism [*McLelland et al*., 2002; *Sepahi et al*., 2004]. Olivine in natural geological settings is commonly associated with Al, Cr suppliers such as pyroxene, spinel, and amphibole that may release Al and Cr during serpentinization. Consequently, serpentinization reactions may proceed at a much faster speed than previously proposed.

Acknowledgments
This work was financially supported by the Natural Science Foundation of China (41603060 and 91328204), China postdoctoral Science Foundation (2015M570735 and 2016T90805), and the Strategic Priority Research Program of the Chinese Academy of Sciences (XDB06030100). We thank T. Ireland for detailed reviews and language checking. We thank J.H. Zhu from the Second Institute of Oceanography, State Oceanic Administration of China, for performing scanning electron microscope imaging. Thanks also to S. Jiang from South China University of Technology for the help during FTIR analyses. Supporting data are included in an SI file.

References

Allen, D. E., and W. E. Seyfried Jr. (2003), Compositional controls on vent fluids from ultramafic-hosted hydrothermal systems at mid-ocean ridges: An experimental study at 400°C, 500 bars, *Geochim. Cosmochim. Acta*, *67*, 1531–1542.

Allen, D. E., and W. E. Seyfried Jr. (2004), Serpentinization and heat generation: Constraints from lost City and rainbow hydrothermal systems, *Geochim. Cosmochim. Acta*, *68*, 1347–1354.

Andreani, M., I. Daniel, and M. Pollet-Villard (2013), Aluminum speeds up the hydrothermal alteration of olivine, *Am. Mineral.*, *98*, 1738–1744.

Avrami, M. (1939), Kinetics of phase change. I general theory, *J. Chem. Phys.*, *7*, 1103–1112.

Bach, W., H. Paulick, C. J. Garrido, B. Ildefonse, W. P. Meurer, and S. E. Humphris (2006), Unraveling the sequence of serpentinization reactions: Petrology, mineral chemistry, and petrophysics of serpentinites from MAR 15°N (ODP Leg 209, Site 1274), *Geophys. Res. Lett.*, *33*, L13306, doi:10.1029/2006GL025681.

Beard, J. S., B. R. Frost, P. Fryer, A. McCaig, R. Searle, B. Ildefonse, P. Zinin, and S. K. Sharma (2009), Onset and progression of serpentinization and magnetite formation in olivine-rich troctolite from IODP Hole U1309D, *J. Petrol.*, *50*, 387–403.

Beeson, M. H., and E. D. Jackson (1969), Chemical composition of altered chromites from the Stillwater Complex, Montana, *Am. Mineral.*, *54*, 1084–1100.

Berndt, M. E., D. E. Allen, and W. E. Seyfried Jr. (1996), Reduction of CO_2 during serpentinization of olivine at 300°C and 500 bar, *Geology*, *24*, 351–354.

Brazelton, W. J., M. O. Schrenk, D. S. Kelley, and J. A. Baross (2006), Methane- and sulfur-metabolizing microbial communities dominate the Lost City hydrothermal field ecosystem, *Appl. Environ. Microbiol.*, *72*(9), 6257–6270.

Brazelton, W. J., B. Nelson, and M. O. Schrenk (2010), Metagenomic evidence for H_2 oxidation and H_2 production by serpentinite-hosted subsurface microbial communities, *Front. Microbiol.*, *2*, 1–16.

Burkhard, D. J. M. (1993), Accessory chromium spinels: Their coexistence and alteration in serpentinites, *Geochim. Cosmochim. Acta*, *57*, 1297–1306.

Charlou, J. L., Y. Fouquet, H. Bougault, J. P. Donval, J. Etoubleau, P. Jean-Baptiste, A. Dapoigny, P. Appriou, and P. A. Rona (1998), Intense CH_4 plumes generated by serpentinization of ultramafic rocks at the intersection of the 15°20′N fracture zone and the Mid-Atlantic Ridge, *Geochim. Cosmochim. Acta*, *62*, 2323–2333.

Charlou, J. L., J. P. Donval, Y. Fouquet, P. Jean-Baptiste, and N. Holm (2002), Geochemistry of high H_2 and CH_4 vent fluids issuing from ultramafic rocks at the rainbow hydrothermal field (36°14′N, MAR), *Chem. Geol.*, *191*, 345–359.

Chen, D. G., B. X. Li, and X. C. Zhi (1994), Genetic geochemistry of mantle-derived peridotite xenolith from Panshishan, Jiangsu, *Geochimica*, *23*, 13–24.

Deschamps, F., M. Godard, S. Guillot, C. Chauvel, M. Andreani, K. Hattori, B. Wunder, and L. France (2012), Behavior of fluid-mobile elements in serpentinites from abyssal to subduction environments: Examples from Cuba and Dominican Republic, *Chem. Geol.*, *312-313*, 93–117.

Dungan, M. A. (1979), A microprobe study of antigorite and some serpentine pseudomorphs, *Can. Mineral.*, *17*, 771–784.

Ehlmann, B. L., et al. (2008), Orbital identification of carbonate-bearing rocks on Mars, *Science*, *322*, 1828–1832.

Ehlmann, B. L., et al. (2009), Identification of hydrated silicate minerals on Mars using MRO-CRISM: Geologic context near Nili Fossae and implications for aqueous alteration, *J. Geophys. Res.*, E00D08, *114*, doi:10.1029/2009JE003339.

Ehlmann, B. L., J. F. Mustard, and S. L. Murchie (2010), Geologic setting of serpentine deposits on Mars, *Geophys. Res. Lett.*, *37*, L06201, doi:10.1029/2010GL042596.

Emmanuel, S., and B. Berkowitz (2006), Suppression and simulation of seafloor hydrothermal convection by exothermic mineral hydration, *Earth Planet. Sci. Lett.*, *243*, 657–668.

Escartín, J., G. Hirth, and B. Evans (1997), Effects of serpentinization on the lithosphere strength and the style of normal faulting at low-spreading ridges, *Earth Planet. Sci. Lett.*, *151*, 181–189.

Escartín, J., G. Hirth, and B. Evans (2001), Strength of slightly serpentinized peridotites: Implications for the tectonics of oceanic lithosphere, *Geology*, *29*, 1023–1026.

Evans, B. W., K. Hattori, and A. Baronnet (2013), Serpentinite: What, why, where?, *Elements*, *9*, 99–106.

Farkaš, J., V. Chrastny, M. Novák, E. Čadkova, J. Pašava, R. Chakrabarti, S. B. Jacobsen, L. Ackerman, and T. D. Bullen (2013), Chromium isotope variations ($\delta^{53/52}$Cr) in mantle-derived sources and their weathering products: Implications for environmental studies and the evolution of $\delta^{53/52}$Cr in the Earth's mantle over geologic time, *Geochim. Cosmochim. Acta*, *123*, 74–92.

Foresti, E., M. Gazzano, A. F. Gualtieri, I. G. Lesci, B. Lunelli, G. Pecchini, E. Renna, and N. Roveri (2003), Determination of low levels of free fibres of chrysotile in contaminated soils by X-ray diffraction and FTIR spectroscopy, *Anal. Bioanal. Chem.*, *376*, 653–658.

Foustoukos, D. I., and W. E. Seyfried Jr. (2004), Hydrocarbons in hydrothermal vent fluids: The role of chromium-bearing catalysts, *Science*, *304*, 1002–1005.

Fuchs, Y., J. Linares, and M. Mellini (1998), Mössbauer and infrared spectrometry of lizardite-1T from Monte Fico, Elba, *Phys. Chem. Minerals.*, *26*, 111–115.

Fukuma, K., and D. J. Dunlop (2006), Three-dimensional micromagnetic modeling of randomly oriented magnetite grains (0.03–0.3 μm), *J. Geophys. Res.*, *111*, B12S11, doi:10.1029/2006JB004562.

Ge, K. P., and Q. S. Liu (2014), Effects of the grain size distribution on magnetic properties of magnetite: Constraints from micromagnetic modeling, *Chin. Sci. Bull.*, *59*(34), 4763–4773.

Golightly, J. P., and O. N. Arancibia (1979), The chemical composition and infrared spectrum of nickel and iron-substituted serpentine from a nickeliferous laterite profile, Soroako, Indonesia, *Can. Mineral.*, *17*, 719–728.

Guillot, S., and K. Hattori (2013), Serpentinites: Essential roles in geodynamics, arc volcanism, sustainable development, and the origin of life, *Elements*, *9*, 95–98.
Hamlyn, P. R. (1975), Chromite alteration in the Panton Sill, East Kimberley Region, Western Australia, *Mineral. Mag.*, *40*, 181–192.
Hattori, K. H., and S. Guillot (2003), Volcanic fronts as a consequence of serpentinites dehydration in the fore-arc mantle wedge, *Geology*, *31*, 525–528.
Hébert, R., A. C. Adamson, and S. C. Komor (1990), Metamorphic petrology of ODP Leg 109, Hole 670A serpentinized peridotite: Serpentinization processes at a slow spreading ridge environment, *Proc. Ocean Drill. Program Sci. Results*, *106*(109), 103–115.
Ho, Y. S., and G. McKay (1999), Pseudo-second order model for sorption processes, *Process Biochem.*, *34*, 451–465.
Holm, N. G., and J. L. Charlou (2001), Initial indications of abiotic formation of hydrocarbons in the rainbow ultramafic hydrothermal system. Mid-Atlantic ridge, *Earth Planet. Sci. Lett.*, *191*, 1–8.
Huang, R. F., W. D. Sun, D. Xing, J. Z. Liu, and S. B. Peng (2015), Olivine versus peridotite during serpentinization: Gas formation, *Sci. China Earth Sci.*, *58*(12), 2165–2174.
Huang, R. F., W. D. Sun, J. Z. Liu, X. Ding, S. B. Peng, and W. H. Zhan (2016), The H_2/CH_4 ratio during serpentinization cannot reliably identify biological signatures, *Sci. Rep-UK*, *6*, 33821, doi:10.1038/srep33821.
Huang, R. F., C. T. Lin, W. D. Sun, X. Ding, W. H. Zhan, and J. H. Zhu (2017), The production of iron oxide during peridotite serpentinization: Influence of pyroxene, *Geosci. Front.*, doi:10.1016/j.gsf.2017.01.001.
Hyndman, R. D., and S. M. Peacock (2003), Serpentinization of the forearc mantle, *Earth Planet. Sci. Lett.*, *212*, 417–432.
Iyer, K., L. H. Rüpke, J. P. Morgan, and I. Grevemeyer (2012), Controls of faulting and reaction kinetics on serpentinization and double Benioff zones, *Geochem. Geophys. Geosyst.*, *13*, Q09010, doi:10.1029/2012GC004304.
Jeanloz, R. (1980), Infrared spectra of olivine polymorphs: α, β phase and spinel, *Phys. Chem. Miner.*, *5*, 327–341.
Jones, L. C., R. Rosenbauer, J. I. Goldsmith, and C. Oze (2010), Carbonate control of H_2 and CH_4 production in serpentinization systems at elevated P-Ts, *Geophys. Res. Lett.*, *37*, L14306, doi:10.1029/2010GL043769
Kelley, D. S., et al. (2001), An off-axis hydrothermal vent field near the Mid-Atlantic Ridge at 30°N, *Nature*, *412*, 145–149.
Klein-BenDavid, O., A. M. Logvinova, M. Schrauder, Z. V. Spetius, Y. Weiss, E. H. Hauri, F. V. Kaminsky, N. V. Sobolev, and O. Navon (2009), High-Mg carbonatitic microinclusions in some Yakutian diamonds-a new type of diamond-forming fluid, *Lithos*, *112s*, 648–659.
Klein-BenDavid, O., T. Pettke, and R. Kessel (2011), Chromium mobility in hydrous fluids at upper mantle conditions, *Lithos*, *125*, 122–130.
Lafay, R., G. Montes-Hernandez, E. Janots, R. Chiriac, N. Findling, and F. Toche (2012), Mineral replacement rate of olivine by chrysotile and brucite under high alkaline conditions, *J. Cryst. Growth*, *347*, 62–72.
Lafay, R., G. Montes-Hernandez, E. Janots, R. Chiriac, N. Findling, and F. Toche (2014), Simultaneous precipitation of magnesite and lizardite from hydrothermal alteration of olivine under high-carbonate alkalinity, *Chem. Geol.*, *368*, 63–75.
Lang, S. Q., D. A. Butterfield, M. Schulte, D. S. Kelley, and M. D. Lilley (2010), Elevated concentrations of formate, acetate and dissolved organic carbon found at the Lost City hydrothermal field, *Geochim. Cosmochim. Acta*, *74*, 941–952.
Liu, Q. S., Q. L. Zeng, J. P. Zheng, T. Yang, N. Qiu, Z. F. Liu, Y. H. Luo, and Z. M. Jin (2010), Magnetic properties of serpentinized garnet peridotites from the CCSD main hole in the Sulu ultrahigh-pressure metamorphic belt, eastern China, *J. Geophys. Res.*, *115*, B06104, doi:10.1029/2009JB000814.
Malvoisin, B., F. Brunet, J. Carlut, S. Rouméjon, and M. Cannat (2012a), Serpentinization of oceanic peridotites: 2. Kinetics and progresses of San Carlos olivine hydrothermal alteration, *J. Geophys. Res.*, *117*, B04102, doi:10.1029/2011JB008842.
Malvoisin, B., J. Carlut, and F. Brunet (2012b), Serpentinization of oceanic peridotites: 1. A high-sensitivity method to monitor magnetite production in hydrothermal experiments, *J. Geophys. Res.*, *117*, B01104, doi:10.1029/2011JB008612.
Manning, C. E. (2007), Solubility of corundum + kyanite in H_2O at 700°C and 10 kbar: Evidence for Al-Si complexing at high pressure and temperature, *Geofluids*, *7*, 258–269.
Marcaillou, C., M. Muñoz, O. Vidal, T. Parra, and M. Harfouche (2011), Mineralogical evidence for H_2 degassing during serpentinization at 300°C/300 bar, *Earth Planet. Sci. Lett.*, *303*, 281–290.
Martin, B., and W. S. Fyfe (1970), Some experimental and theoretical observations on the kinetics of hydration reactions with particular reference to serpentinization, *Chem. Geol.*, *6*, 185–202.
McCollom, T. M., and W. Bach (2009), Thermodynamic constraints on hydrogen generation during serpentinization of ultramafic rocks, *Geochim. Cosmochim. Acta*, *73*, 865–875.
McCollom, T. M., K. Frieder, M. Robbins, B. Moskowitz, T. S. Berquó, N. Jöns, W. Bach, and A. Templeton (2016), Temperature trends for reaction rates, hydrogen generation, and partitioning of iron during experimental serpentinization of olivine, *Geochim. Cosmochim. Acta*, *181*, 175–200.
McLelland, J., J. Morrison, B. Selleck, B. Cunningham, C. Olson, and K. Schmidt (2002), Hydrothermal alteration of late- to post-tectonic Lyon mountain granitic genesis, Adirondack mountains, New York: Origin of quartz-sillimanite segregations, quartz-albite lithologies, and associated Kiruna-type low-Ti Fe-oxide deposits, *J. Metamorph. Geol.*, *20*, 175–190.
Mellini, M., C. Rumori, and C. Viti (2005), Hydrothermally reset magmatic spinels in retrograde serpentinites: Formation of "ferritchromit" rims and chlorite aureoles, *Contrib. Mineral. Petrol.*, *149*, 266–275.
Mével, C. (2003), Serpentinization of abyssal peridotites at mid-ocean ridges, *Compt. Rendus Geosci.*, *335*, 825–852.
Montes-Hernandez, G., A. Fernández-Martínez, and F. Renard (2009), Novel method to estimate the linear growth rate of submicrometric calcite produced in a triphasic gas-liquid-solid system, *Cryst. Growth Des.*, *9*, 4567–4573.
Moody, J. B. (1976), An experimental study on the serpentinization of iron-bearing olivines, *Can. Mineral.*, *14*, 462–478.
Nisbet, E. G., and C. M. R. Fowler (1996), Some liked it hot, *Nature*, *382*, 404–405.
Normand, C., A. E. Williams-Jones, R. F. Martin, and H. Vali (2002), Hydrothermal alteration of olivine in a flow-through autoclave: Nucleation and growth of serpentine phases, *Am. Mineral.*, *87*, 1699–1709.
Okamoto, A., Y. Ogasawara, Y. Ogawa, and N. Tsuchiya (2011), Progress of hydration reactions in olivine-H_2O and orthopyroxenite-H_2O systems at 250°C and vapor-saturated pressure, *Chem. Geol.*, *289*, 245–255.
Salvi, S., G. S. Pokrovski, and J. Schott (1998), Experimental investigation of aluminum-silica aqueous complexing at 300°C, *Chem. Geol.*, *151*, 51–67.
Scambelluri, M., O. Müntener, J. Hermann, G. B. Piccardo, and V. Trommosdorff (1995), Subduction of water into the mantle: History of an Alpine peridotite, *Geology*, *23*, 459–462.
Scambelluri, M., E. Rampone, and G. B. Piccardo (2001), Serpentinite: A trace-element study of the Erro-Tobbio high-pressure ultramafites (Western Alps, NW Italy), *J. Petrol.*, *42*, 55–67.
Scambelluri, M., J. Fiebig, N. Malaspina, O. Müntener, and T. Pettke (2004), Serpentinite subduction: Implications for fluid processes and trace-element recycling, *Int. Geol. Rev.*, *46*, 595–613.

Schmidt, M. W., and S. Poli (1998), Experimentally based water budgets for hydrating slabs and consequences for arc magma generation, *Earth Planet. Sci. Lett.*, *163*, 361–379.
Schrenk, M. O., D. S. Kelley, S. A. Bolton, and J. A. Baross (2004), Low archaeal diversity linked to subseafloor geochemical processes at the Lost City hydrothermal field, mid-Atlantic ridge, *Environ. Microbiol.*, *6*(10), 1086–1095.
Schrenk, M. O., W. J. Brazelton, and S. Q. Lang (2013), Serpentinization, carbon, and deep life, *Rev. Mineral. Geochem.*, *75*, 575–606.
Sepahi, A. A., D. L. Whitney, and A. A. Baharifar (2004), Petrogenesis of andalusite-kyanite-sillimanite veins and host rocks, Sanandaj-Sirjan metamorphic belt, Hamadan, Iran, *J. Metamorph. Geol.*, *22*, 119–134.
Seyfried, W. E., Jr., D. I. Foustoukos, and Q. Fu (2007), Redox evolution and mass transfer during serpentinization: An experimental and theoretical study at 200°C, 500 bar with implications for ultramafic-hosted hydrothermal systems at mid-ocean ridges, *Geochim. Cosmochim. Acta*, *71*, 3872–3886.
Seyfried, W. E., Jr., N. J. Pester, K. Ding, and M. Rough (2011), Vent fluid chemistry of the Rainbow hydrothermal system (36°N, MAR): Phase equilibria and in situ pH controls on subseafloor alteration processes, *Geochim. Cosmochim. Acta*, *75*, 1574–1593.
Seyler, M., M. Cannat, and C. Mével (2003), Evidence for major-element heterogeneity in the mantle source of abyssal peridotites from the southwest Indian ridge (52° to 68°E), *Geochem. Geophys. Geosyst.*, *4*(2), 9101, doi:10.1029/2002GC000305.
Sleep, N. H. (2010), The Hadean-Archaean environment. Cold spring Harb, *Perspect. Biol.*, *2*(6), a002527.
Smirnov, A. V. (2009), Grain size dependence of low-temperature remanent magnetization in natural and synthetic magnetite: Experimental study, *Earth Planets Space*, *61*, 119–124.
Sun, W. D., Z. C. Peng, X. C. Zhi, D. G. Chen, Z. R. Wang, and X. H. Zhou (1998), Osmium isotope determination on mantle-derived peridotite xenoliths from Panshishan with N-TIMS, *Chin. Sci. Bull.*, *43*, 573–575.
Ulmer, G. C. (1974), Alteration of chromite during serpentinization in the Pennsylvania-Maryland District, *Am. Mineral.*, *59*, 1236–1241.
Ulmer, P., and V. Trommsdorff (1995), Serpentine stability to mantle depths and subduction-related magmatism, *Science*, *268*, 858–861.
Wegner, W. W., and W. G. Ernst (1983), Experimentally determined hydration and dehydration reaction rates in the system MgO-SiO_2-H_2O, *Am. J. Sci.*, *283-A*, 151–180.
Xu, X. S., W. L. Griffin, S. Y. OReilly, N. J. Pearson, H. Y. Geng, and J. P. Zheng (2008), Re-Os isotopes of sulfides in mantle xenoliths from eastern China: Progressive modification of lithospheric mantle, *Lithos*, *102*, 43–64.
Yang, X. Y. (2008), Geochemical study on Cenozoic mantle derived peridotitic xenoliths from Panshishan and Lianshan, Jiangsu Province, Master thesis, 23 pp., Guangzhou Institute of Geochemistry, Chinese Academy of Sciences.
Zahnle, K., N. Arndt, C. Cockell, A. Halliday, E. Nisbet, F. Selsis, and N. H. Sleep (2007), Emergence of a habitable planet, *Space Sci. Rev.*, *129*, 35–78.